Growth kinetics of core-shell-structured grains and dielectric constant in rare-earth-doped $BaTiO_3$ ceramics

Gang Liu, Xiao-hui Wang, Y. Lin, L.-T. Li, and Ce-Wen Nan

Citation: Journal of Applied Physics **98**, 044105 (2005); doi: 10.1063/1.2030413
View online: http://dx.doi.org/10.1063/1.2030413
View Table of Contents: http://aip.scitation.org/toc/jap/98/4
Published by the American Institute of Physics

Growth kinetics of core-shell-structured grains and dielectric constant in rare-earth-doped $BaTiO_3$ ceramics

Gang Liu, Xiao-hui Wang,[a] Y. Lin, L.-T. Li, and Ce-Wen Nan[b]
State Key Laboratory of New Ceramics and Fine Processing, and Department of Materials Science and Engineering, Tsinghua University, Beijing 100084, China

(Received 1 December 2004; accepted 10 July 2005; published online 23 August 2005)

The solute-drag-dependent growth kinetics of core-shell-structured grains in rare-earth-doped $BaTiO_3$ ceramics was studied based on an analytical description of the diffusion of rare-earth atoms doped. Dependence of the sizes of grain core and shell on the sintering conditions, dopant content, and starting powder size was quantitatively revealed. The effective dielectric constant of the ceramics was calculated in terms of the relative contents of the ferroelectric core and paraelectric shell. The calculations are in good agreement with the experimental observations. © *2005 American Institute of Physics*. [DOI: 10.1063/1.2030413]

I. INTRODUCTION

$BaTiO_3$ is one of the most important ceramics for ceramic capacitor applications. For $BaTiO_3$ ceramics used in multiplayer ceramic capacitors, it has been known that a high dielectric constant and good temperature stability can be achieved through the addition of dopants such as rare-earth (Re) atoms, which results in core-shell-structured grains after sintering,[1] as typically shown in Fig. 1. The core is nearly free from dopants and retains as ferroelectric phase, while the shell is paraelectric because the solid solution of dopants in $BaTiO_3$ reduces the Curie temperature.[2–4] Accordingly, the effective dielectric properties of Re-doped $BaTiO_3$ are closely dependent on the volume fractions of the ferroelectric core and the paraelectric shell. As a result, the grain size R and the shell size l [see Fig. 1(b)] are two crucial parameters for the core-shell-structured $BaTiO_3$ ceramics, which reflect the relative content of the two constituent phases.

The grain size in the $BaTiO_3$ ceramic is controlled not only by the particle size of starting $BaTiO_3$ powder but also by the grain growth process during its sintering. In pure and homogenous $BaTiO_3$, the grain growth is driven by boundary curvatures without pinning effect on boundary mobility. However, in Re-doped $BaTiO_3$, the grain growth could be inhibited due to drag effect caused by the dopant atoms distributing on the outer layer of the grains.[5,6] It has been suggested that the drag force is proportional to the difference between dopant atom concentrations in the grain exterior region and in the interior region.[7–9] Of practical interest, the kinetics of the grain growth in Re-doped $BaTiO_3$ is then mainly dominated by the diffusion-dependent dopant atom distributions. The shell size is essentially equivalent to the width of the region over which the dopant atoms distribute,[4,10,11] as shown in Fig. 1(c). Thus the diffusion and distribution of the dopant atoms play an important role in affecting the growth kinetics of such core-shell-structured grains and thereby the effective dielectric constant. However, there is still lack of comprehensive fundamental understanding of these issues.

In this paper, on the basis of an analytical description of the diffusion of the dopant atoms, the solute-drag-dependent growth kinetics of the core-shell-structured $BaTiO_3$ grains of nano-and submicrosize is investigated. The grain size, shell size, and volume fractions of constituent core and shell regions are found to be dependent on sintering conditions, dopant content, and starting particle size. In addition, the grain-size-dependent dielectric constant is calculated for the doped $BaTiO_3$. All the predictions are agreeable with the experimental results.

II. THEORETICAL FRAMEWORK

Assume that the additives are homogenously aggregated at the surface of the $BaTiO_3$ powder after ball milling. During sintering, the dopant atoms diffuse into the interior grain driven by the chemical-potential difference. This results in a gradient distribution of the dopant atom concentration c which can be described by Fick's second law as

$$\frac{\partial c}{\partial t} = D\frac{\partial^2 c}{\partial x^2}, \tag{1}$$

where t is the diffusion time or sintering duration, x is the distance away from the grain surface to the interior grain, and D is the diffusion coefficient of the dopant atom and expressed as

$$D = D_0 \exp\left(-\frac{Q_d}{kT}\right), \tag{2}$$

where D_0 is a preexponential factor, Q_d is the activation energy of diffusion, k is the Boltzman constant, and T is the absolute sintering temperature. The solution of Eq. (1) is written as

[a]Electronic mail: wxh@mail.tsinghua.edu.cn
[b]Author to whom correspondence should be addressed; electronic mail: cwnan@mail.tsinghua.edu.cn

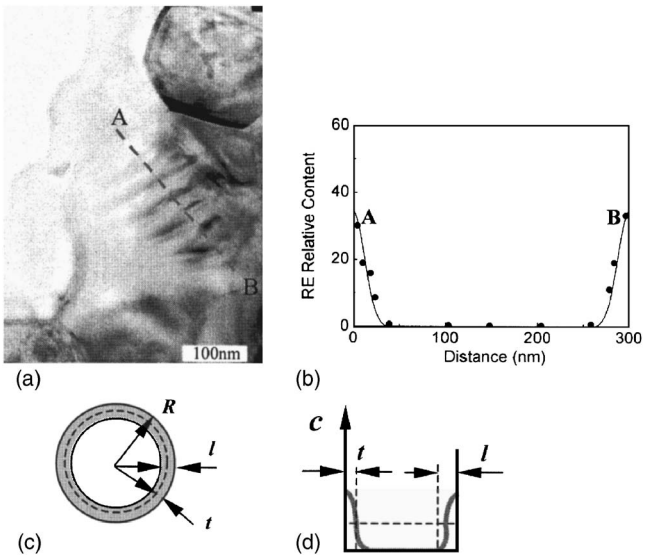

FIG. 1. (a) Typical TEM image of the core-shell-structured grains in Sm-doped $BaTiO_3$ ceramics sintered at 1200 °C for 2 h. (b) Measured profile of Re relative content in the same core-shell grain continuously from A to B as marked in (a). Schematic illustration of (c) a core-shell-structured grain and (d) the distribution of dopant atoms over the core-shell-structured grain as well as the definition of l and t.

$$c(x,t) = \frac{m}{\sqrt{\pi D t}} \exp\left(-\frac{x^2}{4Dt}\right), \tag{3}$$

where m is the amount of the additive per unit area initially distributed on the surface of the $BaTiO_3$ powder and can be obtained as

$$m = \rho_m \bar{R} w / 3M(1-w), \tag{4}$$

where w is the dopant content (at. %), M and ρ_m are the molecular weight and density of $BaTiO_3$, respectively, and $\bar{R}$ is the average radius of the starting powder $\bar{R}_0$. From Eq. (3), the shell size l could be approximately determined from $c(l,t)=0$.

At the same time, the growth kinetics of the core-shell-structured grains could be described as[7]

$$\frac{d\bar{R}}{dt} = A\left(\frac{\alpha\gamma}{\bar{R}} - F\right), \tag{5}$$

where α is a geometric factor close to unity, A and γ are the grain-boundary mobility $[A=A_0 \exp(-Q_v/kT)]$ and grain-boundary energy, respectively, and F is the solute-drag force that is proportional to both the grain-boundary velocity and the difference between the exterior and interior solute concentrations $\Delta c(t)$. So Eq. (5) can be rewritten as

$$\frac{d\bar{R}}{dt} = A\left[\frac{\alpha\gamma}{\bar{R}} - \beta\Delta c(t)\frac{d\bar{R}}{dt}\right], \tag{6}$$

with β being a scaling factor. $\Delta c(t)$ is determined by

$$\Delta c(t) = \bar{c}_{\text{ext}}(t) - \bar{c}_{\text{int}}(t) = \frac{1}{l}\int_0^l c(t)dx, \tag{7}$$

where $\bar{c}_{\text{ext}}(t)$ is the average solute concentration at the outer grain part or at the shell part and $\bar{c}_{\text{int}}(t)$ is that at the central grain part or at the core part $[\bar{c}_{\text{int}}(t)\approx 0]$. The integration of Eq. (5) yields

$$(\bar{R}^2 - \bar{R}_0^2) + A\beta[\bar{R}^2\Delta c(t) - \bar{R}_0^2\Delta c(0)] = A\gamma t. \tag{8}$$

This equation shows that the evolution of the grain size is related to sintering temperature, sintering duration, starting powder size, and dopant content.

III. EXPERIMENT

Ultrafine $BaTiO_3$ powders with different average starting powder sizes, i.e., $\bar{R}_0$=15, 40, 60, 125, and 180 nm, were prepared by oxalate precipitation method.[12] A small amount of 0.5-at. % Sm_2O_3 was added into all these $BaTiO_3$ powders. The ceramic samples were prepared by a solid-state procedure[12] such as sintering at 1200–1280 °C for 1–2 h. The microstructure of the ceramic samples was observed by using a HITACHI S450 scanning electron microscope (SEM), and a transmission electron microscope (TEM, JEM-2010F, Japan) with an energy-dispersive x-ray spectroscopy (EDS) was employed to observe the core-shell structure and to analyze the chemical compositions.[13] The room-temperature dielectric constant of the ceramics was measured using a HP 4194A LR impedance analyzer.

IV. RESULTS AND DISCUSSION

A. Growth of the core-shell structure

Figure 1(a) shows a typical TEM image of the core-shell grains observed in the Sm-doped $BaTiO_3$ ceramics, where the core is the ferroelectric phase and the shell is the paraelectric phase. The ferroelectric domains are clearly seen at the core part while absent at the shell part. Further compositional measurement reveals that the concentration of rare-earth element Sm decreases gradually from the outer shell to the inner shell and down to zero at the core part, as shown in Fig. 1(b). Phenomenally, the shell size l is approximately equal to the diffusion length [Figs. 1(c) and 1(d)], in good agreement with others' results.[4,10,11] This grain-boundary size might also be described in terms of a half width at half maximum of the concentration, t [see Figs. 1(c) and 1(d)]. However, the volume fraction as well as the dielectric property of the paraelectric shell is more associated with the parameter l rather than t. Therefore, the shell size l is used in the present paper.

Figure 2 shows a typical comparison between TEM photographs of starting $BaTiO_3$ powders ($\bar{R}_0$=40 nm) and of grains of the sintered ceramic, both in a same magnification. An obvious growth of the grains is observed by comparing the microstructural features before and after sintering, although the growth process is also inhibited by the drag effect caused by the dopant atoms distributing on the outer layer of the grains. From Fig. 2(b), it seems that the paraelectric shell would be inhomogeneous and somewhat varies in thickness,

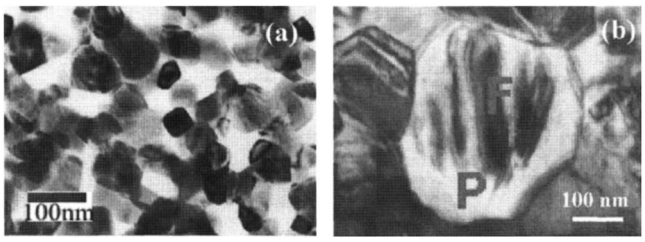

FIG. 2. A typical TEM photograph of (a) the $BaTiO_3$ powder of $\bar{R}_0$ =40 nm and (b) the sintered ceramics at 1200 °C for 2 h.

which is mainly due to microstructural inhomogeneities before sintering. The shell size l calculated by using the average grain size $\bar{R}$ denotes an average boundary thickness.

Figure 3 shows the influence of sintering temperature and sintering duration on the relative concentration of Sm atoms, i.e., Sm/(Ba+Ti), over a grain boundary of the core-shell structure from the starting powder size of $\bar{R}_0$=125 nm. The lines are the calculated results and the dots are the measured results for the samples sintered at different sintering temperatures with different sintering durations. The calculations from the present model are performed by using the values for the parameters listed in Table I. The comparison demonstrates that the calculations are in quite good agreement with the experimental data. Both the increase in sintering temperature and the prolongation in sintering duration promote the diffusion of Sm atoms and thus expand the width of Sm-rich region, which results in an increase in the shell size. As seen from Fig. 4, when the sintering temperature increases from 1200 to 1250 °C, the shell size will increase by about 20 nm, with an increasing percentage larger than 50% [Fig. 4(a)]. In comparison, the increasing percentage with the sintering duration is somewhat lower [Fig. 4(b)], so the sintering duration exerts a less influence on the shell growth than the sintering temperature.

TABLE I. Parameters used in the present calculations (see Refs. 14 and 15).

Parameters	Expression or values
D (m^2/s)	$6.31\times10^{-5}\exp(-4.35/kT)$
A (m^2/s)	$9.52\times10^{9}\exp(-7.87/kT)$[a]
γ (J/m^2)	1.5

[a]Calibrated from the present experimental results.

Presented in Fig. 5 is the dependence of the grain growth on the sintering temperature, sintering duration, and starting $BaTiO_3$ powder size. The comparison also illustrates a good match between the calculations and experiments. The grain size largely increases with the sintering temperature [Fig. 5(a)], but slowly grows after a long sintering duration of about 0.5 h, especially at low sintering temperature [Fig. 5(b)].

Besides the sintering conditions, the starting $BaTiO_3$ powder size $\bar{R}_0$ also plays an important role in controlling the final grain size. Figure 5(c) shows that the grain size $\bar{R}$ in the sintered ceramics is proportional to the starting $BaTiO_3$ powder size $\bar{R}_0$. This tendency is similar to the experimental observations by Park and Kim,[4] where another rare-earth oxide, Ce_2O_3, was doped into the $BaTiO_3$ to form a similar core-shell structure.

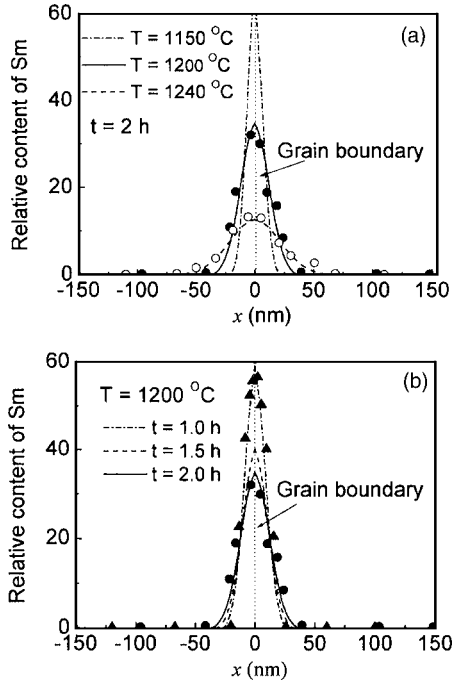

FIG. 3. Dependence of relative concentration, Sm/(Ba+Ti), of Sm atoms over a grain boundary of the core-shell structure on (a) sintering temperature and (b) sintering duration. The curves are the calculated results and the close dots, open dots, and triangle dots are the experimental data for the Sm-doped $BaTiO_3$ ceramics sintered at 1200 °C for 2 h, at 1240 °C for 2 h, and at 1200 °C for 1 h, respectively, from starting powder size of $\bar{R}_0$=125 nm.

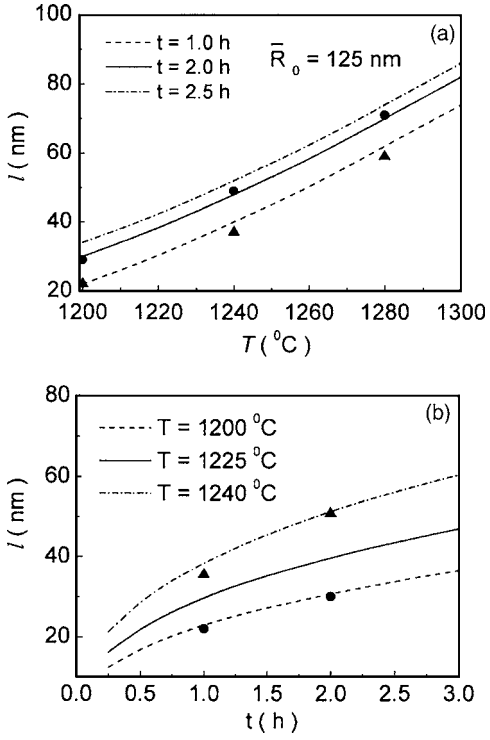

FIG. 4. Dependence of the shell size on (a) sintering temperature and (b) sintering duration. The close and triangle dots in (a) are the experimental data for the ceramics sintered at 1200, 1240, and 1280 °C for 1 and 2 h, respectively. The close and triangle dots in (b) are the experimental data for the ceramics sintered at 1200 and 1240 °C, respectively, for 1 and 2 h.

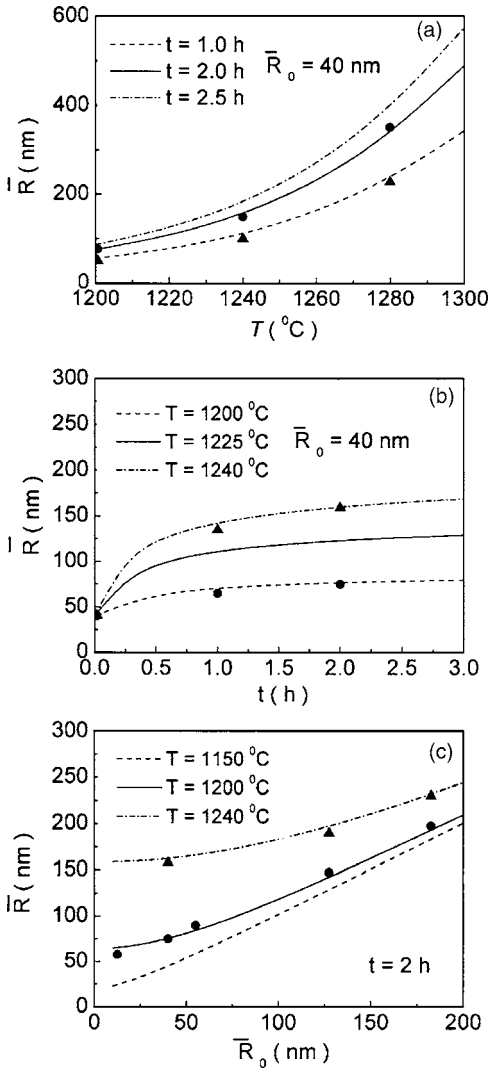

FIG. 5. Dependence of the grain size on (a) sintering temperature, (b) sintering duration, and (c) starting powder size $\bar{R}_0$. The close and triangle dots in (a) are the experimental results for the Sm-doped $BaTiO_3$ ceramics sintered at 1200, 1240, and 1280 °C for 1 and 2 h respectively. The close and triangle dots in (b) are the experimental results for the ceramics sintered at 1200 and 1240 °C, respectively, for 1 and 2 h. The dots in (c) are the experimental results for the ceramics sintered at 1200 °C for 2 h with starting powder sizes of $\bar{R}_0$=15, 40, 60, 125, and 180 nm, respectively.

B. Dielectric constant

During sintering, the grain growth is accompanied by the shell growth. The relative contents or volume fractions of the core ferroelectric phase and the shell paraelectric phase are dependent on the sintering conditions and the starting powder size. Thus the effective dielectric constant of the core-shell-structured $BaTiO_3$ is dependent on these influence parameters as well.

Figure 6(a) shows the calculated and measured dependences of the volume fraction f of the core ferroelectric phase on the sintering duration as a function of the sintering temperature T. Both the elevated sintering temperature and the prolonged sintering duration are favorable for increasing the content of the ferroelectric core phase due to much larger increase in $\bar{R}$ (Fig. 5) than in the shell size l (Fig. 4). Ac-

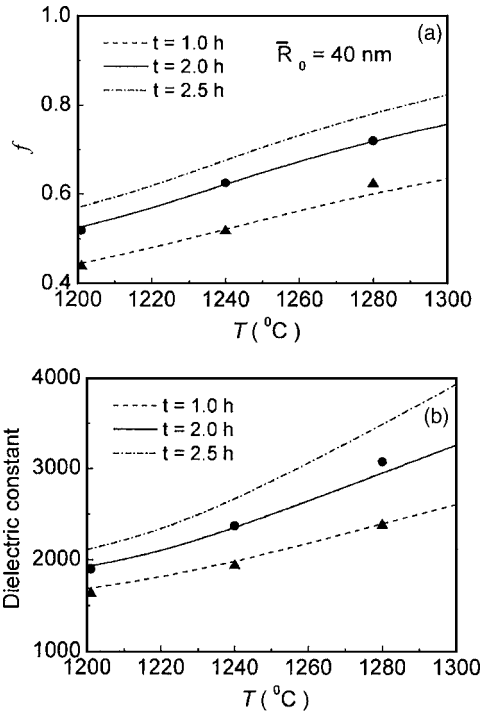

FIG. 6. Effect of the sintering duration on (a) the volume fraction f of the core ferroelectric phase and (b) the effective dielectric constant of the Sm-doped $BaTiO_3$ ceramics as a function of sintering temperature. The close and triangle dots are the experimental results of the ceramics sintered at 1200, 1240, and 1280 °C for 1 and 2 h, respectively, from starting powder of $\bar{R}_0$=40 nm.

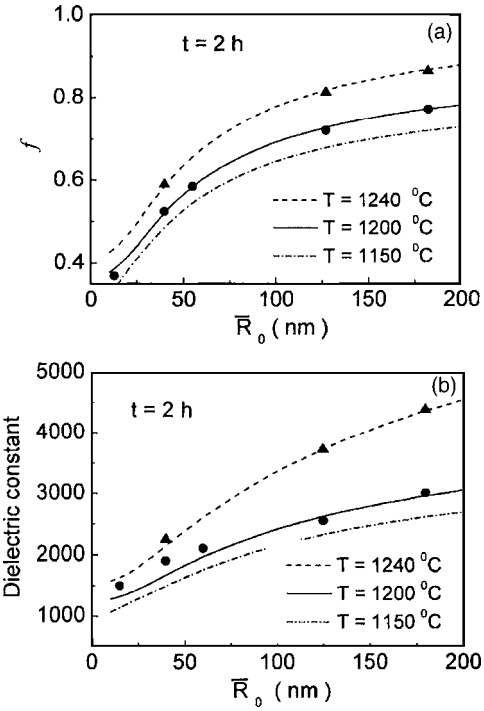

FIG. 7. Effect of the starting powder size on (a) the volume fraction of the core ferroelectric phase and (b) effective dielectric constant of the Sm-doped $BaTiO_3$ ceramics. The close and triangle dots are the experimental results of the ceramics sintered at 1200 and 1240 °C, respectively, for 2 h.

cording to the well-known Maxwell-Garnett approximation,[16] the effective dielectric constant can be expressed as

$$\varepsilon = \varepsilon_{she}\left(1 + \frac{3f\beta}{1 - f\beta}\right), \tag{9}$$

where $\beta = (\varepsilon_{cor} - \varepsilon_{she})/(\varepsilon_{cor} + 2\varepsilon_{she})$, and ε_{cor} and ε_{she} are the dielectric constants of the ferroelectric core and paraelectric shell, respectively. The dielectric constant of the Sm-doped $BaTiO_3$ ceramics should increase with f. If one takes the intrinsic ε_{cor} as 3200 and ε_{she} as 800,[10] the calculated relationship between ε and T is depicted as in Fig. 6(b). Similarly, Figs. 7(a) and 7(b) show the calculated and measured dependences of f and ε on the starting powder size $\bar{R}_0$, respectively. A larger starting powder size would result in a higher content of ferroelectric core phase [Fig. 7(a)] and therefore produce a larger dielectric constant [Fig. 7(b)]. It is seen that the calculations are also in agreement with the experimental results.

The value of ε_{cor} in the calculations above is taken as 3200, which is somewhat larger than that for pure $BaTiO_3$ ceramics in the case of submicron-sized grains.[17] However, this value is reasonable for the core region in the present case. This is mainly attributed to the strong constraint effect in the core-shell structures. As the core region is ferroelectric at room temperature, a phase transformation from paraelectric to ferroelectric will occur at the Curie temperature during the cooling process from sintering temperature and thus spontaneous electrostrictive deformation is due for the core region. By contrary, the shell region is paraelectric and undergoes no phase transformation. Correspondingly, the shell region will be out of coincidence with the core region in elastic deformation. As a result, the outer shell region would exert constraints on the deforming core region, which induces a strong internal stress in the ferroelectric core region. The elastic Gibbs energy for the core ferroelectric phase derived from the cubic phase under isothermal conditions may be expressed in the classic Landau-Ginsburg-Devonshire (LGD) phenomenological thermodynamic theory as[18–20]

$$\begin{aligned}\Delta G = {} & \alpha_1(P_1^2 + P_2^2 + P_3^2) + \alpha_{11}(P_1^4 + P_2^4 + P_3^4) + \alpha_{12}(P_1^2P_2^2 + P_1^2P_3^2 + P_2^2P_3^2) + \alpha_{111}(P_1^6 + P_2^6 + P_3^6) + \alpha_{112}[P_1^4(P_2^2 + P_3^2) + P_2^4(P_1^2 \\ & + P_3^2) + P_3^4(P_1^2 + P_2^2)] + \alpha_{123}P_1^2P_2^2P_3^2 - \tfrac{1}{2}s_{11}(X_1^2 + X_2^2 + X_3^2) - s_{12}(X_1X_2 + X_2X_3 + X_3X_1) - \tfrac{1}{2}s_{44}(X_4^2 + X_5^2 + X_6^2) - Q_{11}(X_1P_1^2 \\ & + X_2P_2^2 + X_3P_3^2) - Q_{12}[X_1(P_2^2 + P_3^2) + X_2(P_1^2 + P_3^2) + X_3(P_1^2 + P_2^2)] - Q_{44}(P_2P_3X_4 + P_1P_3X_5 + P_1P_2X_6),\end{aligned} \tag{10}$$

where ΔG is the Gibbs free function for unit area; α_i, α_{ij}, and α_{ijk} are the dielectric stiffness and higher-order stiffness coefficients at constant stress, among which α_1 and α_{11} are temperature dependent for $BaTiO_3$;[21] X_i is the internal stress in the ferroelectric core region, s_{ij} is the elastic compliance coefficient, and Q_{ij} is the electrostrictive constant in polarization notation. Following the treatment of Pertsev *et al.*,[21] the mechanical conditions in present case are $\partial\Delta G/\partial X_1 = \partial\Delta G/\partial X_2 = -u_1$, $\partial\Delta G/\partial X_3 = -u_3$, and $\partial\Delta G/\partial X_4 = \partial\Delta G/\partial X_5 = \partial\Delta G/\partial X_6 = 0$, where u_1 and u_3 are the deformation strains in phase transformation along $a(b)$ axis and c axis, respectively, with $u_1 = (a - a_0)/a_0$ and $u_3 = (c - a_0)/a_0$. Here a and c are the lattice constants of the tetragonal $BaTiO_3$ and a_0 is the constant of cubic $BaTiO_3$; $a = 0.3992$ nm, $c = 0.403\,61$ nm, and $a_0 = 0.400\,66$ nm. According the LGD phenomenological theory, the dielectric constants of the tetragonal $BaTiO_3$ single grain are related to the inverse of the second derivation of ΔG [Eq. (10)] with respect to the polarization component P_i of the ferroelectric phase,[22,23] i.e.,

$$\varepsilon_{33} = \left(\frac{\partial^2\Delta G}{\partial P_3^2}\right)^{-1}, \quad \varepsilon_{11} = \left(\frac{\partial^2\Delta G}{\partial P_1^2}\right)^{-1}. \tag{11}$$

Finally, for the ferroelectric core in the $BaTiO_3$ ceramics, the dielectric constant is averaged as[24]

$$\varepsilon_{cor} = \frac{1}{4}(\varepsilon_{11} + \sqrt{\varepsilon_{11}^2 + 8\varepsilon_{11}\varepsilon_{33}}). \tag{12}$$

Based on the aforementioned mechanical conditions and by using the values for these parameters listed in Table II, the value of ε_{cor} is evaluated as 3158, close to 3200 that we used above.

It should be pointed out that some similar increases in the dielectric constant caused by the internal stress in $BaTiO_3$ have been reported in the literature.[25–27] However, the internal stress in the present case is induced by the con-

TABLE II. Properties of $BaTiO_3$ used in the present LGD calculations (see Ref. 21).

Parameters	Expression or values
α_1 (V m/C)	$3.3(T-110)\times10^{5}$[a]
α_{11} (V m^5/C^3)	$3.6(T-175)\times10^{6}$
α_{111} (V m^9/C^5)	6.6×10^{9}
α_{12} (V m^5/C^3)	4.9×10^{8}
α_{112} (V m^9/C^5)	2.9×10^{9}
Q_{11} (m^4/C^2)	0.11
Q_{12} (m^4/C^2)	−0.043
S_{11} (10^{12} m^2/N)	8.1
S_{12} (10^{12} m^2/N)	−3.5

[a] T is 25 °C in the present case.

straint effect from the outer region on the interior region, which is the characteristic of the core-shell structures in doped $BaTiO_3$ ceramics.

V. CONCLUSIONS

The solute-drag dependence of grain growth in Re-doped $BaTiO_3$ ceramics has been studied based on the analytical description of the diffusion of dopant atoms. The growth kinetics of the core-shell structures has been quantitatively presented, from which the dependence of the grain and shell sizes on the sintering temperature, sintering duration, dopant content, and starting powder size has been revealed. The calculated grain growth is in agreement with the experimental observations. Based on the description of the grain growth, the relative volume fractions of the ferroelectric core region and the paraelectric shell region have been evaluated and the effective dielectric constant of the ceramics have been calculated, which is roughly agreeable with the measured values.

ACKNOWLEDGMENTS

This work was supported by the State Key Project of Fundamental Research of China (Grant Nos. 2002CB613301 and 2002CB613303) and NSF of China. Experimental work was done by one of the author's (X.W.) group supported by Grant No. 2002CB613301.

[1]B. S. Rawal, K. Manfred, and W. R. Buessem, in *Grain Boundary Phenomena in Electronic Ceramics*, Advances in Ceramics Vol. 1 (American Ceramic Society, Columbus, OH, 1981), p. 172.
[2]D. Henning and G. Rosentein, J. Am. Ceram. Soc. **67**, 249 (1984).
[3]T. R. Armstrong, L. E. Morgens, A. K. Maurice, and R. C. Buchanan, J. Am. Ceram. Soc. **72**, 605 (1989).
[4]Y. Park and H. G. Kim, J. Am. Ceram. Soc. **80**, 106 (1997).
[5]J. W. Chan, Acta Metall. **10**, 789 (1962).
[6]M. Hillert, Acta Metall. **13**, 227 (1965).
[7]E. Rabkin, Scr. Mater. **42**, 1199 (2000).
[8]A. Michels, C. E. Krill, H. Ehrhardt, R. Birringer, and D. T. Wu, Acta Mater. **47**, 2143 (1999).
[9]R. Kirchheim, Acta Mater. **50**, 413 (2002).
[10]H. Chazono and H. Kishi, J. Am. Ceram. Soc. **83**, 101 (2000).
[11]S. H. Yoon, J. H. Lee, and D. Y. Kim, J. Am. Ceram. Soc. **85**, 3111 (2002).
[12]X. H. Wang, R. Z. Chen, Z. L. Gui, and L. T. Li, Mater. Sci. Eng., B **B99**, 199 (2003).
[13]R. Z. Chen, X. H. Wang, L. T. Li, and Z. L. Gui, Key Eng. Mater. **224**, 37 (2002).
[14]J. A. Orman, T. L. Grove, and N. Shimizu, Contrib. Mineral. Petrol. **141**, 687 (2001).
[15]G. A. Chadwick and D. A. Smith, *Grain Boundary Structure and Properties* (Academic, New York, 1976).
[16]C. W. Nan, Prog. Mater. Sci. **37**, 1 (1993).
[17]S. H. Wemple, M. Didomenico, Jr., and I. Camlible, J. Phys. Chem. Solids **29**, 1797 (1968).
[18]A. F. Dovenshire, Philos. Mag. **40**, 1040 (1949).
[19]A. Amin, M. J. Haun, B. Badger, H. Mckinstry, and L. E. Cross, Ferroelectrics **65**, 107 (1985).
[20]M. J. Haun, E. Furman, S. J. Jang, and L. E. Cross, Ferroelectrics **99**, 13 (1989).
[21]N. A. Pertsev, A. G. Zembilgotov, and A. K. Tagantsev, Phys. Rev. Lett. **80**, 1988 (1998).
[22]Z. G. Ban and S. P. Alpay, Appl. Phys. Lett. **91**, 9288 (2002).
[23]H. Li, A. L. Roytburd, S. P. Alpay, T. D. Tran, L. Salamanca-Riba, and R. Ramesh, Appl. Phys. Lett. **78**, 2354 (2001).
[24]D. A. G. Bruggeman, Ann. Phys. **24**, 634 (1935).
[25]G. Arlt, D. Hennings, and G. de With, J. Appl. Phys. **58**, 1619 (1985).
[26]A. J. Bell, A. J. Moulson, and L. E. Cross, Ferroelectrics **54**, 147 (1984).
[27]J. K. Lee, Y. H. Lee, K. S. Hong, and J. W. Jang, J. Appl. Phys. **95**, 219 (2004).